Structural properties and superconductivity in the ternary intermetallic compounds *MAB* (*M*=Ca, Sr, Ba; *A*=Al, Ga, In; *B*=Si, Ge, Sn)

Michael J. Evans,[1] Yang Wu,[1] Verina F. Kranak,[1] N. Newman,[2] Armin Reller,[3] F. Javier Garcia-Garcia,[3] and Ulrich Häussermann[1]

[1]*Department of Chemistry and Biochemistry, Arizona State University, Tempe, Arizona 85287-1604, USA*

[2]*School of Materials, Arizona State University, Tempe, Arizona 85287-8706, USA*

[3]*Lehrstuhl für Festkörperchemie, Institut für Physik, Universität Augsburg, Universitätsstrasse 1, D-86159 Augsburg, Germany*

(Received 8 April 2009; revised manuscript received 8 July 2009; published 27 August 2009)

The ternary intermetallic compounds *MAB*=CaAlSi, SrAlSi, BaAlSi, CaGaSi, SrGaSi, BaGaSi, SrAlGe, BaAlGe, CaGaGe, SrGaGe, BaGaGe, BaInGe, BaAlSn, CaGaSn, SrGaSn, and BaGaSn have been prepared by arc-melting stoichiometric elemental mixtures and structurally characterized by a combination of x-ray powder and electron diffraction. They crystallize as variants of the simple hexagonal AlB_2 structure type where trivalent and tetravalent *A*- and *B*-type atoms, respectively, form commonly a planar hexagon layer, and structural variations arise from *A*/*B* ordering and/or puckering of hexagon layers. The silicides (*B*=Si) were previously investigated for their superconducting properties. By dc magnetization measurements it is demonstrated that also the germanides SrAlGe, BaAlGe, SrGaGe, and BaGaGe and the stannide BaAlSn are superconductors above 2 K.

DOI: 10.1103/PhysRevB.80.064514 PACS number(s): 74.10.+v, 61.66.Dk, 74.70.Dd, 74.62.Bf

I. INTRODUCTION

The discovery of superconductivity at 39 K in MgB_2 (Ref. 1) has drawn attention to isostructural intermetallic compounds with the simple AlB_2 structure.[2–4] In this respect the ternary silicides *M*AlSi and *M*GaSi (*M*=Ca, Sr, Ba) have been extensively investigated and superconductivity above 2 K has been found for all systems, with the exception of BaAlSi.[5–10] In the ternary systems Si and Al/Ga commonly take the position of the boron atoms forming hexagon layers while *M* atoms occupy the "intercalating" positions. Generally, superconducting critical temperatures, T_c, for the ternary silicides are considerably lower than for MgB_2. The highest T_c is 7.8 K and found for CaAlSi.[11]

Although both types of systems, MgB_2 and *MA*Si (*A*=Al, Ga) are considered as conventional superconductors, their mechanism of electron-phonon coupling is quite different. While the key ingredient to the superconducting properties of MgB_2 are partially occupied B-B σ bonding states that couple strongly to in-plane vibrations of boron,[12] this situation is radically changed for *MA*Si due to the increased electron count (nine valence electrons) and the higher mass of constituting atoms. For *MA*Si, theoretical investigations identified partially occupied π^* and *M*-*d* states in conjunction with a soft mode that is associated with the out-of-plane *A*-Si vibration as the origin for the superconducting properties.[13–17] Recent inelastic neutron and x-ray scattering experiments showed the existence of this soft mode for CaAlSi and confirmed its large anharmonicity and strong electron-phonon coupling.[18,19]

The nine-electron systems *MA*Si can be considered as charge imbalanced (not electron precise) Zintl phases. The electronic structure of a planar hexagon layer formed by main group atoms is characterized by three bonding σ bands. Additionally, the p_z orbitals give rise to two π bands, one bonding and one antibonding. The Zintl concept assumes a formal charge transfer from the electropositive component *M* to the atoms forming the hexagon layer, and for main group AlB_2 systems an electron precise situation with all bonding bands filled is attained in eight-electron systems (e.g., $SrGa_2$ and $BaGa_2$). Puckering of the hexagon layers destroys the π bands and creates more localized (lone pair) electronic states. Arsenic-like layers are electron precise for ten-electron systems and, for instance, realized in the structures of $CaSi_2$ and $CaGe_2$.[20]

The partial filling of the antibonding π^* band in nine-electron AlB_2 systems *MA*Si is thought to be responsible for the soft mode, which expresses an inherent structural instability toward layer puckering.[16,18] Indeed, for CaAlSi polymorphs exhibiting slightly corrugated hexagon layers were identified, and their modulated structures are termed 5H and 6H in the literature (and 1H is used for the planar-layer AlB_2 form).[21] Such structural variations, which have a marked influence on the superconducting properties of CaAlSi,[22–24] have not been reported for SrAlSi, BaAlSi, and *M*GaSi. An additional issue is the degree of ordering of the two different kinds of elements within the hexagon layers. For *M*AlSi the discrimination between Al and Si is difficult to extract from diffraction experiments. Again CaAlSi has been most investigated and ordered and disordered variants have been reported for all polymorphs.[22,25] It appears, however, that ordering within hexagon layers is of minor significance to superconducting properties.

Ternary nine-electron systems are not restricted to silicides but extend to germanides and stannides. Known are the germanides SrAlGe, BaAlGe, CaGaGe, SrGaGe, and BaGaGe and the stannides CaGaSn and SrGaSn.[26–28] While the aluminum compounds adopt the planar-layer AlB_2 structure, the gallium germanides and stannides are all reported with the YPtAs structure consisting of ordered and pronouncedly puckered hexagon layers. It is surprising that hitherto only silicides have been investigated for superconducting properties. Considering also germanides and stannides as potential superconductors, the nine-electron systems *MAB*

(*A*=Al, Ga, In; *B*=Si, Ge, Sn) provide a unique compositional playground—enriched with structural variations—for fundamental studies of electron-phonon coupling phenomena in this class of conventional superconductors. Here we report a comparative study of the structural properties and superconductor behavior (above 2 K) of all possible elemental *MAB* combinations crystallizing as variants of the AlB_2 structure.

II. METHODS

All steps of synthesis and sample preparation for diffraction and electron microcopy experiments were carried out under dry argon. Ca (99.98%), Sr (99.95%), Ba (99.9%), Ga (99.999%), and Ge (99.999%) from Aldrich, and Al (99.99%), In (99.9%), Si (99.999%), and Sn (99.999%) from Alfa Aesar were used as received. The ternary nine-electron compounds *MAB* were prepared by arc-melting stoichiometric mixtures of the pure elements on a water-cooled copper hearth and remelted three times to ensure homogeneity. Due to the volatility of *M* a low current arc was employed. Samples obtained from arc-melting were ground and their phase purity established by powder x-ray diffraction patterns taken on a Siemens D5000 diffractometer (Bragg-Brentano geometry; Cu Kα radiation).

Lattice parameters and atomic positions of the ternary phases *MAB* were determined by Rietveld analysis[29] of high-resolution powder x-ray diffraction data using the TOPAS program.[30] Finely ground samples were measured in 0.1 mm capillaries, and the high-resolution powder x-ray diffraction patterns were taken on a Bruker D8 diffractometer fitted with an incident-beam Ge monochromator (transmission geometry; Cu Kα_1 radiation). For Rietveld analysis, the following parameters were refined: background, unit cell, sample displacement, profile, atomic positions, isotropic atomic displacement parameters, and absorption correction.[31] For some samples, anisotropic peak broadening was modeled using spherical harmonics.[32] Results are compiled in Tables I and II. Due to the large amount of impurities in CaGaSn, Rietveld analysis was not performed on that sample.

Samples for electron microscopy investigations were ground in a mortar and the resulting fine crystallites were supported onto holey-carbon coated copper grids. Transfer of the sample into the sample holder and into the electron microscope was done under normal air conditions. The subsequent transmission electron microscopy studies were carried out in a JEOL JEM-2100 F transmission electron microscope operated at 200 kV and equipped with EDAX detector for compositional analysis. Due to the rapid decomposition of SrAlGe, BaAlGe, BaAlSn, and CaGaSn when exposed to air, investigation of those compounds were not possible.

Temperature-dependent magnetizations of *MAB* samples (with the exception of impure CaGaSn) were measured by the vibrating sample magnetometer (VSM) on a Quantum Design PPMS system. Powdered specimens were placed into a brass trough sample holder and sealed with a small amount of fast-curing superglue under dry argon. Subsequently the sample holder was loaded vertically into the PPMS chamber. Transition temperatures T_c were determined with magnetization measurements from 15 to 2 K at a rate of 1 K/min. The magnetic field was calibrated with $Gd_2(SO_4)_3 \cdot 8H_2O$, a paramagnetic standard with a susceptibility of 0.0533 cm^3/mol at room temperature.[33] Zero field cooling (ZFC) and field cooling (FC) measurements under a magnetic field of around 10 Oe were conducted for samples showing saturated magnetization above 2 K. Magnetization curves (*M* vs *H*) were taken for SrAlGe and BaAlGe at 3 K on the same PPMS. Applied magnetic fields were up to 1000 Oe at a scanning rate of 10.5 Oe/s. The minima of the increase field part of the magnetization curves correspond to the lower critical field, H_{c1}, typically found for type-II superconductors.

Theoretical calculations were performed in the framework of the frozen-core all-electron projected augmented wave (PAW) method,[34] as implemented in the program VASP.[35] The energy cutoff was set to 500 eV. Exchange and correlation effects were treated by the generalized gradient approximation (GGA), usually referred to as PW91.[36] The integration over the Brillouin zone was done on special *k* points determined according to the Monkhorst-Pack scheme.[37] Total energies were converged to at least 1 meV/atom. For all *MAB* combinations the unit-cell parameters of the ordered AlB_2 type structure (space group $P\bar{6}m2$) were optimized for a fixed volume of the unit cell. By repeating this process for different volumes the optimum cell parameters are determined from the global minimum energy.

III. RESULTS AND DISCUSSION

Arc-melting of stoichiometric elemental mixtures of *M*, *A*, and *B* affords the compounds *M*AlSi, *M*GaSi, *M*GaGe, and *M*GaSn as well as SrAlGe, BaAlGe, BaInGe, and BaAlSn. Thus our synthesis attempts extend the previously known systems with the new compositions BaGaSn, BaInGe, and BaAlSn. According to x-ray powder-diffraction analysis *MAB* compounds are obtained phase pure with the exception of CaGaSn and SrGaSn samples, which contained a substantial amount of an unidentified side product. Therefore both compounds were also prepared from stoichiometric elemental mixtures that were sealed in niobium ampoules, heated to 1373 K for 8 h and subsequently cooled to room temperature at a rate of 40 K/h. This resulted in a phase pure sample SrGaSn, which was then employed in the further investigations. For CaGaSn no improvement was observed and accordingly we excluded this compound in the further studies. The sensitivity of powder samples *MAB* toward air and moisture is different. Silicides are rather stable while stannides and especially the germanides SrAlGe, BaAlGe, and BaInGe decompose rapidly when exposed to air/moisture. Gallium germanides *M*GaGe behave intermediate and react slowly with air/moisture.

A. Structural properties

The AlB_2 structure and its variants relevant for ternary nine-electron systems *MAB* are compiled in Fig. 1. A detailed overview of structures which can be derived from the AlB_2 type by group-subgroup symmetry relations has been given by Hoffmann and Pöttgen.[38] In the simple AlB_2 type

TABLE I. Crystal data and refinement results for *MAB*. Asterisks denote that compounds actually occur in a modulation of the specified structure type. Note: $R_p=\Sigma|Y_{o,m}-Y_{c,m}|/\Sigma Y_{o,m}$; $R_{wp}=\sqrt{\Sigma w_m(Y_{o,m}-Y_{c,m})^2/\Sigma w_m Y_{o,m}^2}$; $R_B=\Sigma|I_{`o',k}-I_{c,k}|/\Sigma I_{`o',k}$; where $Y_{o,m}$ and $Y_{c,m}$ are the observed and calculated data at point m, respectively, $w_m=1/\sigma(Y_{o,m})^2$, and $I_{`o',k}$ and $I_{c,k}$ are the "observed" and calculated intensities of k^{th} reflection, respectively.

	CaAlSi	SrAlSi	BaAlSi	SrAlGe	BaAlGe
Space group	*P*6/*mmm*	*P*6/*mmm*	*P*6/*mmm*	$P\bar{6}m2$	$P\bar{6}m2$
Structure type	AlB_2^*	AlB_2	AlB_2	SrPtSb	SrPtSb
a, Å	4.1860(1)	4.2433(1)	4.3001(1)	4.3043(1)	4.3512(1)
c, Å	4.3972(1)	4.7435(1)	5.1438(1)	4.7407(1)	5.1401(1)
V, Å^3	66.73(1)	73.97(1)	82.37(1)	76.07(1)	84.28(1)
Z	1	1	1	1	1
χ^2	1.66	2.26	1.56	1.94	1.16
R_p, %	2.94	4.16	3.91	3.10	2.96
R_{wp}, %	4.20	5.95	5.55	4.85	4.22
R_B, %	2.57	2.07	1.82	2.45	2.47

	CaGaSi	SrGaSi	BaGaSi	CaGaGe	SrGaGe
Space group	*P*6/*mmm*	*P*6/*mmm*	*P*6/*mmm*	$P6_3/mmc$	*P*6/*mmm*
Structure type	AlB_2^*	AlB_2	AlB_2	YPtAs*	AlB_2^*
a, Å	4.1101(1)	4.1835(1)	4.2479(1)	4.2203(1)	4.2718(1)
c, Å	4.4466(1)	4.7422(1)	5.1106(1)	17.2876(2)	4.7179(1)
V, Å^3	65.05(1)	71.88(1)	79.86(1)	266.65(1)	74.56(1)
Z	1	1	1	4	1
χ^2	2.23	1.34	1.26	1.38	1.40
R_p, %	3.97	5.07	3.85	2.34	4.36
R_{wp}, %	6.07	7.03	5.24	3.47	6.27
R_B, %	4.38	1.65	1.77	1.82	2.44

	BaGaGe	SrGaSn	BaGaSn	BaInGe	BaAlSn
Space group	*P*6/*mmm*	$P6_3/mmc$	$P6_3/mmc$	$P\bar{3}m1$	*P*6/*mmm*
Structure type	AlB_2	YPtAs	$CaIn_2$	$EuGe_2^*$	AlB_2
a, Å	4.3351(1)	4.5505(1)	4.5807(1)	4.5709(3)	4.6331(1)
c, Å	5.0947(1)	18.710(1)	10.3303(3)	5.0994(3)	5.1408(1)
V, Å^3	82.92(1)	335.53(3)	187.72(1)	92.27(1)	95.57(1)
Z	1	4	2	1	1
χ^2	1.14	2.04	1.22	1.37	1.84
R_p, %	2.19	4.76	3.37	2.90	2.26
R_{wp}, %	3.16	6.98	4.59	4.17	3.53
R_B, %	1.19	1.94	2.00	2.37	4.27

(space group *P*6/*mmm*) *A*- and *B*-type atoms are randomly distributed over the site of the majority atoms forming planar hexagon layers [Fig. 1(a)]. If *A* and *B* atoms are completely ordered in a way that each atom is coordinated by three unlike ones, the AlB_2-type unit cell is maintained but space-group symmetry is reduced to $P\bar{6}m2$. This results in the SrPtSb structure [Fig. 1(b)]. The hexagonal YPtAs structure (space group $P6_3/mmc$) can be regarded as a ternary derivative of the AlB_2-type structure, where puckering of the hexagon layers produces a fourfold superstructure along the *c* direction [Fig. 1(c)]. The puckered hexagon layers are now formed by atoms on two different crystallographic sites. As in the AlB_2 structure, the hexagon layers are stacked on top of each other; however the orientation of layers and distribution of atoms produces an arrangement of double layers where *A*- and *B*-type atoms are located at the inside and outside, respectively.

Most of the previously known systems *MAB* have been described as either planar-layer structured AlB_2 and SrPtSb, or strongly puckered YPtAs. Figure 2 shows representatively the powder x-ray diffraction patterns of BaGaGe (AlB_2 type) and CaGaGe (YPtAs type). Note that the puckering of hexagon layers is pronounced in the YPtAs structure and superstructure reflections (with respect to the AlB_2 type) are easily

TABLE II. Atomic position and isotropic thermal displacement parameters (Å^2).

Compound	Atom	x	y	z	B_{eq}
CaAlSi	Ca	0	0	0	1.27(4)
	Al/Si	1/3	2/3	1/2	2.05(4)
SrAlSi	Sr	0	0	0	0.64(1)
	Al/Si	1/3	2/3	1/2	0.78(3)
BaAlSi	Ba	0	0	0	0.93(6)
	Al/Si	1/3	2/3	1/2	1.11(8)
SrAlGe	Sr	0	0	0	0.29(9)
	Al	1/3	2/3	1/2	1.52(20)
	Ge	2/3	1/3	1/2	0.71(19)
BaAlGe	Ba	0	0	0	0.37(17)
	Al	1/3	2/3	1/2	0.57(48)
	Ge	2/3	1/3	1/2	0.39(32)
CaGaSi	Ca	0	0	0	0.97(5)
	Ga/Si	1/3	2/3	1/2	2.26(4)
SrGaSi	Sr	0	0	0	0.67(3)
	Ga/Si	1/3	2/3	1/2	1.41(4)
BaGaSi	Ba	0	0	0	0.86(8)
	Ga/Si	1/3	2/3	1/2	1.23(9)
CaGaGe	Ca1	0	0	0	0.47(9)
	Ca2	0	0	1/4	1.10(9)
	Ga	1/3	2/3	0.1474(1)	1.53(3)
	Ge	1/3	2/3	0.6150(1)	0.40(2)
SrGaGe	Sr	0	0	0	0.26(2)
	Ga/Ge	1/3	2/3	1/2	1.29(3)
BaGaGe	Ba	0	0	0	0.88(4)
	Ga/Ge	1/3	2/3	1/2	1.57(5)
SrGaSn	Sr1	0	0	0	1.87(14)
	Sr2	0	0	1/4	1.29(12)
	Ga	1/3	2/3	0.1606(2)	1.58(9)
	Sn	1/3	2/3	0.6170(2)	1.34(7)
BaGaSn	Ba	0	0	1/4	0.78(5)
	Ga/Sn	1/3	2/3	0.4802(2)	1.96(6)
BaInGe	Ba	0	0	0	1.47(16)
	In/Ge	1/3	2/3	0.4611(6)	1.39(16)
BaAlSn	Ba	0	0	0	1.22(5)
	Al/Sn	1/3	2/3	1/2	2.20(6)

detectable in powder x-ray diffraction patterns.

The simplest puckered variant of the AlB_2 type, however, is the trigonal $EuGe_2$ structure [Fig. 1(d)], where the layers are formed from one kind of atoms, oriented the same way, and stacked on top of each other along the c direction (space group $P\bar{3}m1$). Note that this stacking of arsenic-like layers is electron precise for ten electron systems. For ordered ternary variants the space-group symmetry will be reduced to $P3m1$ [Fig. 1(e)]. Twofold superstructures along the c direction may arise from an alternate stacking of oppositely oriented puckered hexagon layers [$CaIn_2$ structure, space group $P6_3/mmc$, Fig. 1(f)] or a different distribution of A and B atoms in adjacent planar layers in case of A/B ordering (ZrBeSi type, space group $P6_3/mmc$, not shown) or a combination of different A- and B-type atom distribution and puckering [NdPtSb structure, space group $P6_3mc$, Fig. 1(g)].

Finally, a third group of AlB_2-type derivatives can be identified, which is based on weakly corrugated hexagon layers that produce complicated stacking sequences. This has been found earlier for CaAlSi. The structures of the polymorphs 5H and 6H are shown in Fig. 3. They have been described as commensurately modulated structures within a (3+1)-dimensional formalism assuming randomly disordered A and B atoms,[21] and as conventional superstructures with Al and Si ordered hexagon layers.[25] In the course of this study more examples *MAB* displaying modulations from presumably weakly corrugated layers have been identified. Such modulations are hardly detectable in (in-house) powder x-ray

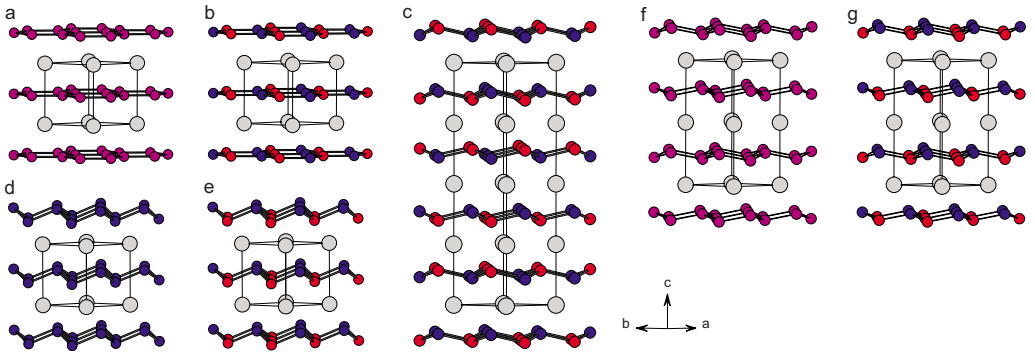

FIG. 1. (Color online) (a) The AlB_2-type structure and some variants: (b) SrPtSb type, (c) YPtAs type, (d) $EuGe_2$ type, (e) ternary ordered $EuGe_2$ structure, (f) $CaIn_2$ type, and (g) NdPtSb type.

diffraction experiments,[21] but may revel in single-crystal diffraction and especially electron diffraction.

(i) *M*AlSi. CaAlSi, SrAlSi, and BaAlSi have been investigated extensively over the recent years.[5,6,9–11] Powder x-ray diffraction patterns show only peaks corresponding to the hexagonal lattice of the AlB_2 structure and the lattice parameters (Table I) are in good agreement with previous reports. Electron diffraction studies [Figs. 4(a) and 4(b)] reveal readily the sixfold superstructure for CaAlSi and confirm the AlB_2 structure for SrAlSi and BaAlSi. Sparta *et al.* reported that polycrystalline 6H-CaAlSi forms from rapidly cooled samples.[21] This is the case with arc-melting synthesis and thus it appears reasonable that our CaAlSi sample corresponded to the 6H polymorph. As mentioned earlier, the actual distribution of Al and Si on the hexagon layers is most difficult to establish experimentally. This is even the case when applying neutron diffraction because the scattering lengths of Al and Si differ by only 10%. Although Al and Si may have a tendency to order, it is reasonable to assume that our specimens obtained from high-temperature arc melting are to a large extent Al/Si disordered.

(ii) *M*AlGe. Among systems *M*AlGe only SrAlGe and BaAlGe can be prepared. Both compounds have been reported to crystallize with the planar-layer ordered SrPtPb type.[27,28] This is confirmed by our investigation. Interesting is the pronounced ordering tendency of Al and Ge, which affords the SrPtSb-type samples even from arc melting. Because of the high sensitivity of SrAlGe and BaAlGe toward air/moisture electron microscopy investigations could not be reliably performed.

(iii) *M*AlSn. Among *M*AlSn systems only BaAlSn represents a variant of the AlB_2 structure. The powder x-ray diffraction pattern of BaAlSn is shown in Fig. 5(a). Rietveld refinement yields Al and Sn atoms randomly distributed on the planar hexagon layer, which is surprising when considering that BaAlGe is ordered and that Al and Sn atoms have a rather large size difference.

(iv) *M*GaSi. Like *M*AlSi systems, *M*GaSi ones have been subject to previous investigations.[4,6] Powder x-ray diffraction

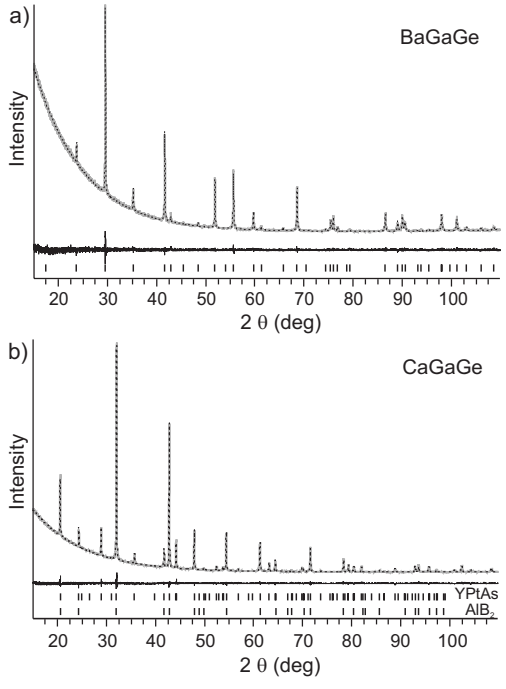

FIG. 2. Rietveld plots for (a) AlB_2-type BaGaGe and (b) YPtAs-type CaGaGe. Gray lines represent the measured powder x-ray pattern, dashed black lines represent the calculated pattern. Bragg-peak positions are marked by horizontal bars. In (b) they are also shown for the AlB_2 basic structure to emphasize the location of peaks arising from the fourfold superstructure, i.e., the YPtAs type.

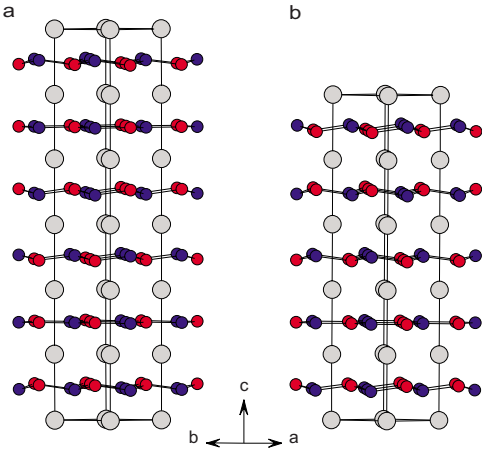

FIG. 3. (Color online) Structures of the (a) 6H and (b) 5H polymorphs of CaAlSi. Gray, red, and blue circles denote Ca (*M*), Al (*A*), and Si (*B*) atoms, respectively.

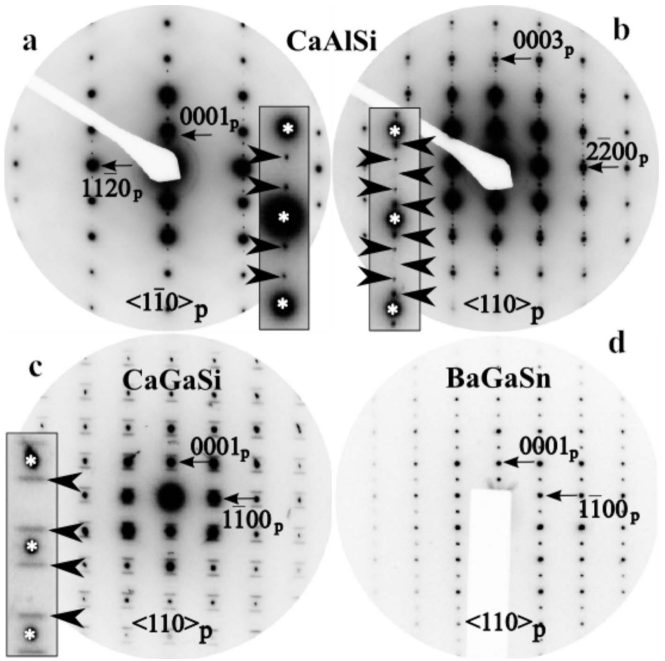

FIG. 4. Collection of relevant zone axis electron-diffraction patterns for the samples CaAlSi, in (a) down $\langle 1\bar{1}0\rangle_p$ and in (b) down $\langle 110\rangle_p$, CaGaSi, in (c) down $\langle 110\rangle_p$, and BaGaSn, in (d) down $\langle 110\rangle_p$. The subscript p indicates indexing according to the parent hexagonal AlB_2 type structure. The magnified areas in (a), (b), and (c) stress deviations from the parent AlB_2 type structure. Note that pattern (a) displays a threefold superstructure that becomes a sixfold superstructure when the crystal is tilted from (a) to (b). Such extinction condition corresponds to the presence of a *c* glide along $[0001]^*$ of the superstructure.

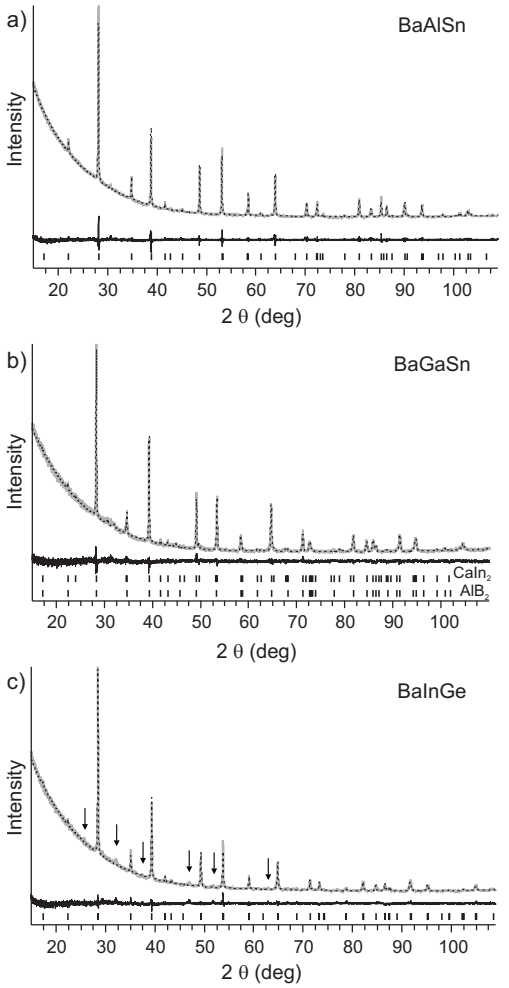

FIG. 5. Rietveld plots for (a) BaAlSn, (b) BaGaSn, and (c) BaInGe. Gray lines represent the measured powder x-ray pattern, dashed black lines represent the calculated pattern. Bragg-peak positions are marked by horizontal bars. BaGaSn, (b), was refined in the $CaIn_2$ structure. The Bragg positions of the AlB_2 basic structure are also shown. Incommensurately modulated BaInGe, (c), was refined in the $EuGe_2$ structure. Weak superstructure reflections are indicated by arrows.

patterns correspond to the hexagonal lattice of the AlB_2-type structure and Rietveld refinements indicate no tendency of Ga/Si ordering, which is in agreement with previous reports.[3] However, for CaGaSi electron diffraction [Fig. 4(c)] shows weak rods of diffuse scattering parallel to $\langle 1\bar{1}00\rangle^*$ and centered at $1/6[0001]^*$. This suggests that Ga/Si atoms are arranged in corrugated layers that produce a sixfold superstructure along the *c* direction [similar to 6H-CaAlSi, cf. Fig. 3(a)], but at the same time there is displacive disorder within the hexagonal *ab* plane. Electron diffraction confirms the AlB_2 structure for SrGaSi and BaGaSi.

(v) *M*GaGe. Gallium germanide compounds have been reported with the puckered-layer ordered YPtAs-type.[26] Our results differ. While powder x-ray diffraction shows clearly the fourfold superstructure for CaGaGe of the YPtAs type [cf. Fig. 2(b)], it is absent for SrGaGe and BaGaGe [cf. Fig. 2(a)] and the latter compounds can be refined in the planar-layer AlB_2 structure. Electron diffraction shows subtle variations for CaGaGe and SrGaGe [Figs. 6(a) and 6(b)]. For CaGaGe, a careful inspection of the zone axis electron-diffraction patterns reveal the existence of an incommensurately modulated structure with $\mathbf{q} \approx (1/4\text{-}\delta)[0001]^*$, where δ is small. (Note that $\delta=0$ gives a $\mathbf{q}$ vector of $(1/4)[0001]^*$, which corresponds to the fourfold commensurate superstructure of the AlB_2-type present in the YPtAs structure.) This peculiarity is also present in the $[1\bar{1}00]$ zone axis where additionally the first-order satellites reflections are absent as a result of the *c* glide along [0001]. For SrGaGe, weak superstructure reflections correspond to a commensurate fivefold superstructure along the hexagonal *c* direction, which resembles the situation of the 5H-CaAlSi structure. BaGaGe was confirmed to possess the lattice of the AlB_2 structure.

(vi) *M*GaSn. CaGaSn and SrGaSn were previously known and reported with the YPtAs structure.[26] This is confirmed in our powder x-ray diffraction patterns and for SrGaSn additionally by electron diffraction. Interestingly, the new compound BaGaSn displays a different structural behavior. At first sight, the analysis of the powder x-ray diffraction pattern yields the AlB_2-type structure for BaGaSn with randomly distributed Ga and Sn atoms [Fig. 5(b)]. However, electron diffraction reveals weak superstructure reflections which correspond to a doubling of the AlB_2 *c* axis [Fig. 4(d)]. This is compatible with two types of puckered hexagon layers that are mutually rotated by 60° (and stacked in "antiphase" ori-

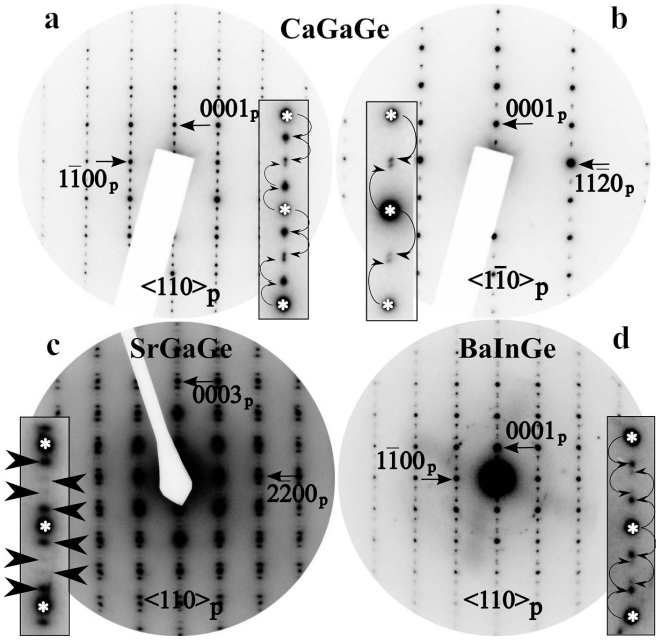

FIG. 6. Collection of relevant zone axis electron-diffraction patterns for the samples CaGaGe, (a) down $\langle 110\rangle_p$ and (b) down $\langle 1\bar{1}0\rangle_p$, SrGaGe, (c) down $\langle 110\rangle_p$, and BaInGe, (d) down $\langle 110\rangle_p$. The subscript p indicates indexing according to the parent hexagonal AlB_2 type structure. Magnified areas of the diffraction patterns stress deviations from the parent AlB_2 type structure. Note that in pattern (a) first- and second-order satellite reflections are present while in (b) only the latter are observed. Such extinction condition corresponds to the presence of a *c* glidelike symmetry relation between the puckering patterns in neighboring layers.

entation). The arrangement is isopointal to ordered NdPtSb or ScAuSi.[38] However, reflection conditions indicate space group $P6_3/mmc$, which implies randomly disordered Ga and Sn. Indeed, a subsequent Rietveld refinement of this structure model from the powder x-ray data leads to a significant improvement over the AlB_2 type (R_{wp}=4.59 vs 5.13 for the former and latter, respectively). Thus BaGaSn should be considered as isostructural to $CaIn_2$ with weakly puckered hexagon layers [cf. Fig. 1(f)].

(vii) *M*InGe. In contrast to the manifold of *MAB* systems which exists with *A*=Al, Ga, only one indium compound can be prepared, BaInGe. This compound has not been reported previously. Powder x-ray diffraction indicates the presence of a superstructure with respect to an AlB_2-type lattice [Fig. 5(c)]. Indeed, electron diffraction [Fig. 6(d)] reveals clearly satellite reflections corresponding to a wave vector $\mathbf{q}=(1/3-\delta)[0001]^*$ and the structure of BaInGe displays actually an incommensurately modulated corrugation of the hexagon layers. This corrugation appears to be rather pronounced. Rietveld refinement of the basic structure from the powder x-ray data shows a clear tendency for hexagon layer puckering (cf. Table II; R_{wp}=4.17 vs 4.59 for puckered and flat layer structure, respectively) and a random distribution of In and Ge atoms on these layers. This corresponds to the $EuGe_2$ structure [cf. Fig. 1(d)].

In conclusion, ternary nine-electron systems *MAB* offer a wide variety in terms of chemical compositions. The basic crystal structures are the disordered AlB_2 and the ordered SrPtSb structure, both based on planar hexagon layers, and the ordered puckered-layer YPtAs structure. Apart from them, subtle variations occur, which originate from various degrees of layer corrugations and/or ordering of *A* and *B* atoms. Those variations represent commensurately and incommensurately modulated superstructures with respect to the AlB_2 type and may be considered as intermediates between the planar-layer and strongly puckered-layer border cases. The ordering tendency of *A*- and *B*-type atoms within hexagon layers varies. Interestingly, it seems to be most pronounced for the pair Al and Ge. However, this should depend on the thermal history of the samples and in this respect no investigations were performed within this study. Also, the occurrence of polymorphism most likely correlates to the thermal history, which could explain that by arc melting we obtained SrGaGe and BaGaGe with a different crystal structure compared to the previously reported one.

The only flexible parameter of the simple AlB_2 structure is the c/a ratio. The *c* parameter is especially affected by the size of the *M* component. For Ca compounds this parameter is between 4.3 and 4.45 Å, whereas for Sr and Ba compounds the range is 4.68–4.78 Å and 5.1–5.15 Å, respec-

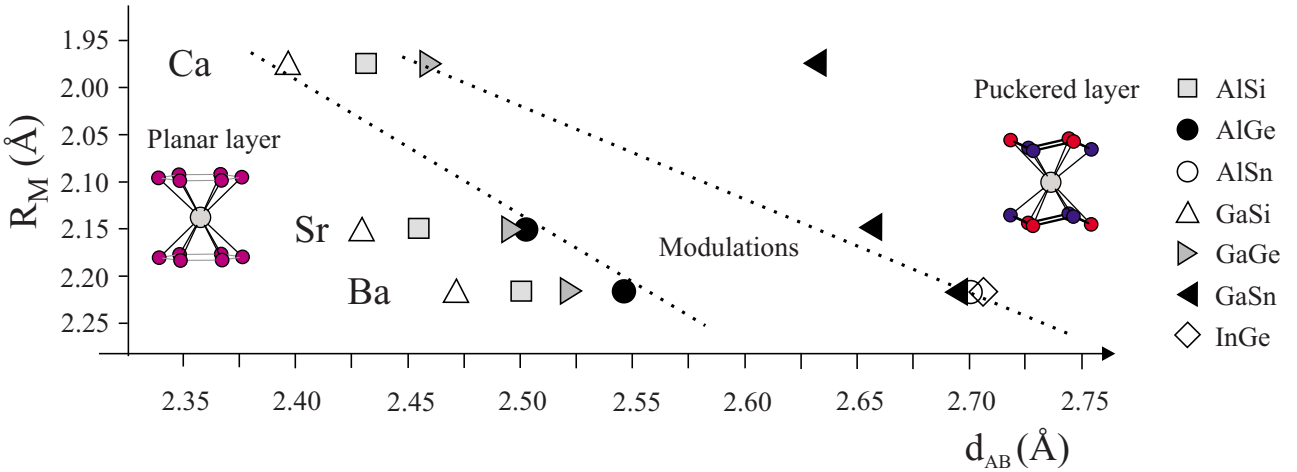

FIG. 7. (Color online) Empirical structure map for *MAB* systems based on the size of *M* [metallic radius according to Pauling (Ref. 39)] and the distribution of *A*-*B* bond lengths assuming all systems are in the planar-layer SrPtSb structure type.

tively (cf. Table I). The *a* parameter is certainly also affected by *M*, but mostly determined by the length of the *A*-*B* bond. In this respect simple geometrical considerations may be used to establish empirically the stability of planar-layer structures AlB_2 and SrPtPb versus the puckered variants. In the AlB_2-type structure the *M* component is sandwiched in between two *AB* hexagon rings. If the rings become too large for coordinating *M* atoms, puckering is induced. We computed the equilibrium lattice parameters for all *MAB* systems in the SrPtSb structure by first-principles calculations (cf. Sec. II) and extracted the *A*-*B* bond length. In those cases where *MAB* actually adopts the AlB_2 or SrPtSb structure (cf. Table I), the calculated distance deviated at the most by 1% from the experimental one.

Figure 7 shows the distribution of computed *A*-*B* distances for each *M*. Additionally, the different *M* series are separated according to the metallic radius of *M* (Ca =1.97 Å, Sr=2.15 Å, Ba=2.21 Å).[40] It is apparent that combinations *A*=Al, Ga with *B*=Si, Ge result in rather similar *A*-*B* distances, while introducing *A*=In or *B*=Sn elongates them considerably. The shortest distance occurs for the pair Ga-Si, the longest for In-Ge. For short *A*-*B* distances typically the planar-layer structure is realized. However, for small-sized *M*=Ca even CaGaSi appears modulated. Further, the puckered YPtAs structure is already adopted in CaGaGe although the modulation we identified there (cf. Fig. 6) may indicate that it is not fully expressed yet. For medium-sized *M*=Sr the boundaries are shifted. SrGaSi and SrAlSi clearly have a planar-layer structure, while modulations appear for SrGaGe and the puckered YPtAs structure for SrGaSn. Finally, for large-sized *M*=Ba there is a large number of representatives with a planar-layer structure and apparently no pair *AB* can afford a distance large enough for inducing the YPtAs structure. Perhaps BaInGe is close to realizing the YPtAs structure, as indicated by the strongly corrugated layer refined for the basic structure (cf. Table II). Figure 7 suggests that the kind of AlB_2-type variant a system *MAB* adopts is related to the ratio of the size of *M* and the size of the coordinating *AB* hexagon ring. The indicated boundaries separating the three fields of structures are not precisely defined. BaAlSn would fall in the field of modulated structures while it was found to adopt the planar-layer AlB_2 structure. However, electron diffraction, which could not be performed here, may actually reveal a modulated structure. Finally we note that the empirical relation established in Fig. 7 are not restricted to *MAB* main group systems but extends to EuGa*B* and to the recently characterized system $Eu(Zn_{1-x}Ge_x)_2$.[39,41]

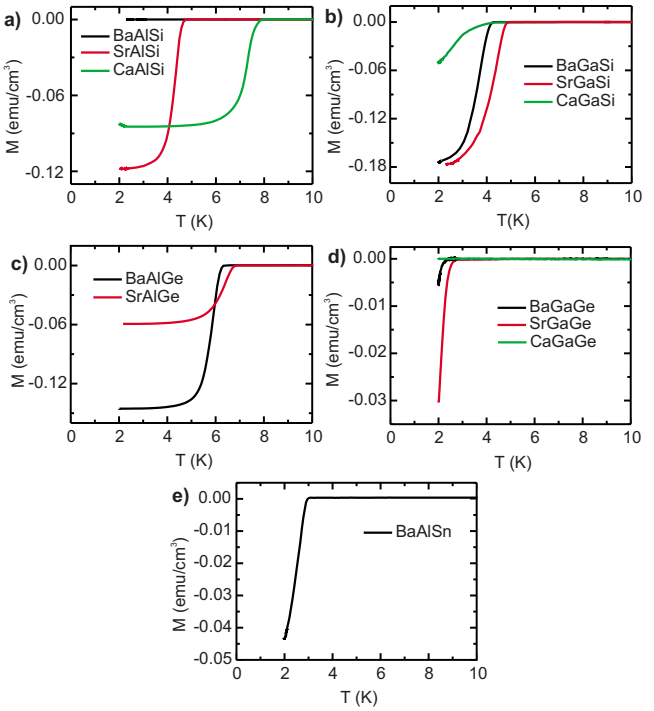

FIG. 8. (Color online) Magnetization (*M*) versus temperature (field cooling) for nine-electron systems (a) *M*AlSi, (b) *M*GaSi, (c) SrAlGe and BaAlGe, (d) *M*GaGe, and (e) BaAlSn.

B. Magnetic susceptibility

Figure 8 shows the temperature dependence of the dc magnetization for systems *MAB*. Additionally the onsets of superconducting critical temperatures, T_c, are compiled in Table III. The superconducting properties of silicides *M*AlSi and *M*GaSi [Figs. 8(a) and 8(b)] have been extensively investigated since the year 2001.[5–11] The polymorphs of CaAlSi—1H, 5H, 6H—have a distinctively different T_c. Our measurement shows a T_c at 7.8 K, in close agreement to what has been reported for the 6H polymorph.[22] Further, we obtain a T_c of 4.7 K for SrAlSi, which is similar to what has been reported in the literature (4.2 and 5.1 K) and confirm the absence of superconductivity above 2 K for BaAlSi.[10] Also for *M*GaSi our values for T_c (4.4, 4.9, and 4.2 K for *M* =Ca, Sr, Ba, respectively) are similar to earlier reports.[4,6]

TABLE III. Superconducting critical temperatures (T_c) of compounds *MAB*. A dash means that no superconductivity was observed above 2 K.

Compound	T_c (K)	Compound	T_c (K)	Compound	T_c (K)
CaAlSi	7.8	CaGaSi	4.4	CaGaSn	–
SrAlSi	4.7	SrGaSi	4.9	SrGaSn	–
BaAlSi	–	BaGaSi	4.2	BaGaSn	–
SrAlGe	6.7	CaGaGe	–	BaInGe	–
BaAlGe	6.3	SrGaGe	2.6		
BaAlSn	2.9	BaGaGe	2.4		

Here we note that the trend of T_c for the series MGaSi is different compared to MAlSi: CaGaSi has a lower T_c than SrGaSi, and BaGaSi is superconducting above 2 K but not BaAlSi. The reason for this different behavior is not clear. The superconductivity of the silicides MAlSi and MGaSi is of type-II. We performed ZFC and FC measurements for CaAlSi, SrAlSi, SrGaSi, and BaGaSi where magnetization saturates above 2 K. The obtained magnetic shielding fractions in ZFC and flux exclusions in FC at 2 K were in agreement with earlier reports.[5–11]

It is interesting now to look at the superconducting behavior of the germanide and stannide systems. Here we find SrAlGe and BaAlGe superconducting at 6.75 and 6.25 K, respectively [Fig. 8(c)]. These are after CaAlSi the highest T_c values among nine-electron MAB systems. It can be speculated that CaAlGe may even display a higher T_c if accessible by synthesis. Furthermore, SrGaGe and BaGaGe are superconductors [Fig. 8(d)], but now T_c is considerably lower compared to aluminum germanides (2.6 and 2.4 K for M =Sr, Ba, respectively). CaGaGe, with the puckered-layer YPtAs structure, is not superconducting above 2 K. The same holds for BaInGe and the gallium stannides MGaSn, which crystallize with either the YPtAs structure or a modulated AlB_2 variant with substantial layer corrugation (e.g., BaInGe). Finally BaAlSn displays superconductivity above 2 K [Fig. 8(e)]. The T_c, however, is fairly low, 2.9 K, especially when compared to BaAlGe (T_c=6.3 K). Due to their low T_c values the magnetization of SrGaGe, BaGaGe, and BaAlSn does not saturate above 2 K and we are not able to rigorously proof that superconductivity in these compounds is a bulk effect. However, the absence of (crystalline) impurities in the x-ray powder patterns indicates bulk superconductivity. Also superconductivity originating from traces of metallic elements and/or alloys can be excluded. For BaAlSn the transition temperature is rather different from that of elemental Sn (3.72 K). Also, Al is only slightly soluble in Sn, with a maximum solubility of about 0.7 at. % Al and this is found to have little effect on the transition temperature.[42]

The rather high T_c values of SrAlGe and BaAlGe allowed for a more detailed characterization of their superconducting properties. Figure 9 shows the dc magnetization of SrAlGe and BaAlGe in ZFC and FC. In FC a Meissner effect (flux exclusion) occurs. The magnetic shielding fraction in ZFC exceeds 90% of the theoretical value of perfect diamagnetism $(1/4\pi)$ at 2 K for both compounds.[43] The flux exclusion in FC at 2 K is about 10% for SrAlGe and about 50% for BaAlGe. This confirms that SrAlGe and BaAlGe are bulk superconductors. The dc magnetization as a function of the magnetic field (insets in Fig. 9) shows type-II behavior with a lower critical field (H_{c1}) around 100 Oe and an upper critical field above 1000 Oe.

In conclusion, we find that superconductivity in ternary nine-electron systems MAB is not restricted to silicides but extends to germanides and stannides. The occurrence of superconductivity clearly relates to the planarity of AB hexagon layers: A transition above 2 K is absent in AlB_2-type variants where layers are substantially puckered (YPtAs-type stannides, $CaIn_2$-type BaGaSn, and incommensurately modulated BaInGe). This, however, remains the only obvious correlation between structural and superconducting properties. For modulated AlB_2 variants with weakly corrugated hexagon layers, the structural influence to T_c is more complex. For instance, T_c is markedly different for the different polymorphs of CaAlSi, but varies irregularly as a function of the c translational period: 1H—6.5 K, 5H—5.7 K, 6H—7.7 K. Furthermore, while the planarity of AB hexagon layers appears to be a necessary condition for superconductivity above 2 K it is by no means sufficient. For the planar-layer systems MAlSi it has been speculated that T_c correlates with the c/a ratio of the AlB_2 structure, and the missing superconductivity of BaAlSi is a consequence of a too large c/a ratio.[10] However, for MGaSi this hypothesis does not apply.

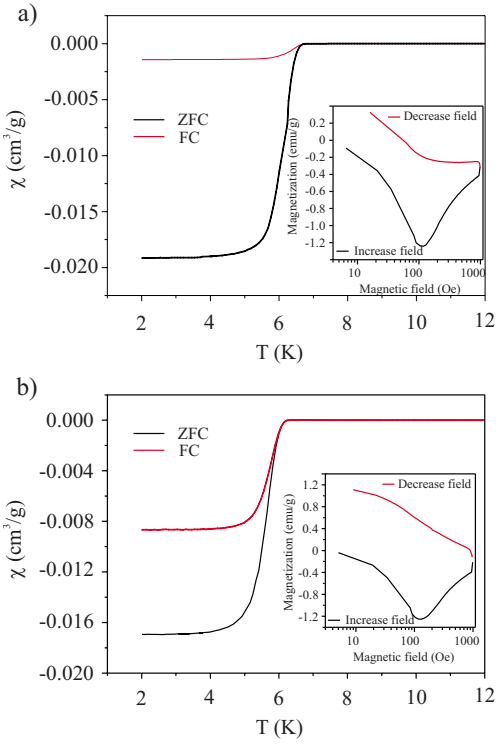

FIG. 9. (Color online) Susceptibility of (a) SrAlGe and (b) BaAlGe at 10 Oe as a function of temperature (zero-field cooling—ZFC, field cooling FC). The insets show the magnetization of SrAlGe and BaAlGe at 3 K as a function of magnetic field.

When attempting to correlate elemental composition of MAB systems with superconductivity perhaps a general trend is that within an M-series Ba compounds will show the lowest T_c, or are even not superconducting above 2 K, and T_c is always high for A=Al compounds. The latter observation contradicts the earlier made assumption that silicon is the major prerequisite for superconductivity in nine-electron MAB systems. While it has been shown that A/B ordering is of minor importance to superconducting properties for silicides (MAlSi and MGaSi) (Refs. 16 and 22) it may be important for germanides and stannides. Here we are not able to draw conclusions.

The present understanding of superconductivity in nine-electron systems MAB is that a low-frequency mode associated with the out-of-plane phonons (optic B_{1g} and acoustic A_{2u} at Γ with respect to the $P6/mmm$ AlB_2 structure), which is soft in the upper half of the Brillouin zone (i.e., the boundary $k_z=\pi/a$), couples to the Fermi-level electrons in the par-

tial occupied π^* band situated at the same location of the Brillouin zone.[14–17] Additionally a second band crossing the Fermi level, that has M-dz^2 character, is important. The presence of the soft mode has been shown by theoretical calculations for the AlB_2-type systems MAlSi and MGaSi, and explicitly confirmed by inelastic neutron and x-ray scattering experiments for 1H-CaAlSi.[18,19] Our findings cast a number of questions:

(1) The soft mode is apparently still present in the modulated layer AlB_2 variants displaying superconductivity. A recent theoretical analysis of the phonon dispersion of 5H- and 6H-CaAlSi found that the soft mode of the 1H polymorph, although due to zone folding now representing a branch, is virtually unchanged by the modulated corrugation of hexagon layers.[24] This is not necessarily expected if the soft mode for 1H-CaAlSi, as speculated in Ref. 18, expresses a structural instability toward layer corrugation or puckering, which then actually occurs in the 5H and 6H polymorphs. So, how will the soft mode change when going to the more strongly puckered AlB_2-type variants and finally the YPtAs structure? How susceptible is the soft mode to compositional variations in A and B?

(2) How is the π^* band developing as a function of composition, hexagon layer separation, and layer puckering? This band has its major contribution from A-type atom p_z orbitals. Is there anything special for A=Al explaining the generally higher T_c values for aluminum compounds? Answering these questions should provide a deeper insight into the electron-phonon coupling mechanism in nine-electron ternary systems MAB.

IV. CONCLUSIONS

The ternary nine-electron intermetallics systems MAB (M=Ca, Sr, Ba; A=Al, Ga, In; B=Si, Ge, Sn) offer a wide variety in terms of chemical compositions. Many silicides (B=Si) have been identified earlier as superconductors above 2 K. MAB compounds crystallize with the simple hexagonal AlB_2 structure or some variant of it. The variations manifest as an ordering of A and B atoms, a puckering of the hexagon layers, or both. The presence and degree of puckering appears to be related to the ratio of the size of M (atomic or ionic radius) and the size of the hexagon ring in the layers as defined by the distance between A and B atoms. When the rings become too large for coordinating M atoms, puckering of the layers is induced. A large size mismatch results in the YPtAs-type structure where AB layer puckering is most pronounced.

Superconductivity in nine-electron MAB systems is not just restricted to aluminum and gallium silicides, but also extends to germanides (SrAlGe, BaAlGe, SrGaGe, BaGaGe) and even stannides (BaAlSn). A prerequisite for superconductivity above 2 K is the presence of planar or weakly corrugated hexagon layers. Superconductivity is clearly absent in representatives with the puckered-layer YPtAs structure. Furthermore, it appears that T_c is lowest or nonexistent above 2 K in a series MAB when M=Ba, and is highest when A=Al (with the notable exception of BaAlSi). The manifold of representatives makes the nine-electron systems MAB a unique playground for further investigations of compositional and structural variations to electron-phonon coupling phenomena in this class of conventional superconductors.

ACKNOWLEDGMENTS

This work has been supported by National Science Foundation under Grants No. DMR-0638826 and No. CHE-CRIF 0742006. We thank Ralph Chamberlin (ASU) for supplying us with $Gd_2(SO_4)_3 \cdot 8H_2O$.

[1] J. Nagamatsu, N. Nakagawa, T. Muranaka, Y. Zenitani, and J. Akimitsu, Nature (London) **410**, 63 (2001).
[2] M. Imai, E. Abe, J. Ye, K. Nishida, T. Kimura, K. Honma, H. Abe, and H. Kitazawa, Phys. Rev. Lett. **87**, 077003 (2001).
[3] R. L. Meng, B. Lorenz, Y. S. Wang, J. Cmaidalka, Y. Y. Sun, Y. Y. Xue, J. K. Meen, and C. W. Chu, IEEE Trans. Appl. Supercond. **13**, 3042 (2003).
[4] R. L. Meng, B. Lorenz, Y. S. Wang, J. Cmaidalka, Y. Y. Sun, Y. Y. Xue, J. K. Meen, and C. W. Chu, Physica C **382**, 113 (2002).
[5] M. Imai, K. Nishida, T. Kimura, and H. Abe, Appl. Phys. Lett. **80**, 1019 (2002).
[6] M. Imai, K. Nishida, T. Kimura, H. Kitazawa, H. Abe, H. Kito, and K. Yoshii, Physica C **382**, 361 (2002).
[7] B. Lorenz, J. Lenzi, J. Cmaidalka, R. L. Meng, Y. Y. Sun, Y. Y. Xue, and C. W. Chu, Physica C **383**, 191 (2002).
[8] B. Lorenz, J. Cmaidalka, R. L. Meng, and C. W. Chu, Phys. Rev. B **68**, 014512 (2003).
[9] T. Nakagawa, M. Tokunaga, and T. Tamegai, Sci. Technol. Adv. Mater. **7**, S108 (2006).
[10] S. Yamanaka, T. Otsuki, T. Ide, H. Fukuoka, R. Kumashiro, T. Rachi, K. Tanigaki, F. Guo, and K. Kobayashi, Physica C **451**, 19 (2007).
[11] M. Imai, El-Hadi S. Sadki, H. Abe, K. Nishida, T. Kimura, T. Sato, K. Hirata, and H. Kitazawa, Phys. Rev. B **68**, 064512 (2003).
[12] H. J. Choi, D. Roundy, H. Sun, M. L. Cohen, and S. G. Louie, Nature (London) **418**, 758 (2002).
[13] I. R. Shein, N. I. Medvedeva, and A. L. Ivansivskii, J. Phys.: Condens. Matter **15**, L541 (2003).
[14] I. I. Mazin and D. A. Papaconstantopoulos, Phys. Rev. B **69**, 180512(R) (2004).
[15] G. Q. Huang, L. F. Chen, M. Liu, and D. Y. Xing, Phys. Rev. B **69**, 064509 (2004).
[16] M. Giantomassi, L. Boeri, and G. B. Bachelet, Phys. Rev. B **72**, 224512 (2005).
[17] G. Q. Huang, M. Liu, L. F. Chen, and D. Y. Xing, Physica C **423**, 9 (2005).
[18] R. Heid, K.-P. Bohnen, B. Renker, P. Adelmann, T. Wolf, D. Ernst, and H. Schober, J. Low Temp. Phys. **147**, 375 (2007).
[19] S. Kuroiwa, A. Q. R. Baron, T. Muranaka, R. Heid, K.-P.

Bohnen, and J. Akimitsu, Phys. Rev. B **77**, 140503(R) (2008).
[20] P. Villars and L. D. Calvert, *Pearsons Handbook of Crystallographic Data for Intermetallic Compounds*, 2nd ed. (ASM International, Materials Park, OH, 1991).
[21] K. M. Sparta, R. Müller, M. Merz, G. Roth, P. Adelmann, and T. Wolf, Acta Crystallogr., Sect. B: Struct. Sci. **62**, 710 (2006).
[22] S. Kuroiwa, H. Sagayama, T. Kakiuchi, H. Sawa, Y. Noda, and J. Akimitsu, Phys. Rev. B **74**, 014517 (2006).
[23] S. Kuroiwa, A. Nakashima, S. Miyahara, N. Furukawa, and J. Akimitsu, J. Phys. Soc. Jpn. **76**, 113705 (2007).
[24] L. Boeri, J. S. Kim, M. Giantomassi, F. S. Razavi, S. Kuroiwa, J. Akimitsu, and R. K. Kremer, Phys. Rev. B **77**, 144502 (2008).
[25] H. Sagayama, Y. Wakabayashi, H. Sawa, T. Kamiyama, A. Hoshikawa, S. Harjo, K. Uozato, A. K. Ghosh, M. Tokunaga, and T. Tamega, J. Phys. Soc. Jpn. **75**, 043713 (2006).
[26] A. Czybulka, B. Pinger, and H.-U. Schuster, Z. Anorg. Allg. Chem. **579**, 151 (1989).
[27] B. Eisenmann, M. Rhode, M. Wehndorff, and C. Röhr, Z. Anorg. Allg. Chem. **634**, 153 (2008).
[28] M. Wendorff and C. Röhr, Z. Naturforsch., B: Chem. Sci. **62**, 1059 (2007).
[29] H. M. Rietveld, J. Appl. Crystallogr. **2**, 65 (1969).
[30] A. X. S. Bruker, *TOPAS V4: General Profile and Structure Analysis Software for Powder Diffraction Data, User's Manual* (Karlsruhe, Germany, 2008).
[31] T. M. Sabine, B. A. Hunter, W. R. Sabine, and C. J. Ball, J. Appl. Crystallogr. **31**, 47 (1998).
[32] M. Järvinen, J. Appl. Crystallogr. **26**, 525 (1993).
[33] K.-H. Hellwege and A. M. Hellwege, *Magnetic and Other Properties of Oxides and Related Compounds*, Landolt-Börnstein, Numerical Data and Functional Relationships in Science and Technology, New Series, III/4 (Springer-Verlag, Heidelberg, 1970).
[34] P. E. Blöchl, Phys. Rev. B **50**, 17953 (1994); G. Kresse and D. Joubert, *ibid.* **59**, 1758 (1999).
[35] G. Kresse and J. Hafner, Phys. Rev. B **47**, 558 (1993); G. Kresse and J. Furthmüller, *ibid.* **54**, 11169 (1996).
[36] J. P. Perdew and Y. Wang, Phys. Rev. B **45**, 13244 (1992).
[37] H. J. Monkhorst and J. D. Pack, Phys. Rev. B **13**, 5188 (1976).
[38] R.-D. Hoffmann and R. Pöttgen, Z. Kristallogr. **216**, 127 (2001).
[39] L. Pauling, J. Am. Chem. Soc. **69**, 542 (1947). Although systems *MAB* are rather polar (Zintl phases), metallic radii are better suited than ionic radii to show the size effect of *M* because the kind of coordination of *M* by 12 *A*, *B* atoms is more typical of intermetallic compounds and also an ionic radius for 12-coordintated Ba has not been defined.
[40] T.-S. You, Y. Grin, and G. J. Miller, Inorg. Chem. **46**, 8801 (2007).
[41] T.-S. You, S. Lidin, O. Gourdon, Y. Wu, and G. J. Miller, Inorg. Chem. **48**, 6380 (2009).
[42] J. Bankuti and E. Farkas, Acta Phys. Acad. Sci. Hung. **50**, 177 (1981).
[43] The crystallographic densities of SrAlGe and BaAlGe are 4.011 and 4.618 g/cm^{-3}, respectively (cf. Table I).